BIOCHEMISTRY
including biophysical chemistry & molecular biology
Article

Biochemistry **2011,** *50,* 1723–1730 1723
DOI: 10.1021/bi1018539

Alteration of Hydrogen Bonding in the Vicinity of Histidine 48 Disrupts Millisecond Motions in RNase A[†]

Nicolas Doucet,[‡,⊥] Gennady Khirich,[‡] Evgenii L. Kovrigin,[§] and J. Patrick Loria*[,‡,∥]

[‡]*Department of Chemistry, Yale University, New Haven, Connecticut 06520, United States,* [§]*Department of Biochemistry, Medical College of Wisconsin, Milwaukee, Wisconsin 53226, United States, and* [∥]*Department of Molecular Biophysics and Biochemistry, Yale University, New Haven, Connecticut 06520, United States.* [⊥]*Current address: INRS-Institut Armand-Frappier, Université du Québec, 531 Boulevard des Prairies, Laval, Quebec H7V 1B7, Canada.*

Received November 19, 2010; Revised Manuscript Received January 12, 2011

ABSTRACT: The motion of amino acid residues on the millisecond (ms) time scale is involved in the tight regulation of catalytic function in numerous enzyme systems. Using a combination of mutational, enzymological, and relaxation-compensated ^{15}N Carr−Purcell−Meiboom−Gill (CPMG) methods, we have previously established the conformational significance of the distant His48 residue and the neighboring loop 1 in RNase A function. These studies suggested that RNase A relies on an intricate network of hydrogen bonding interactions involved in propagating functionally relevant, long-range ms motions to the catalytic site of the enzyme. To further investigate the dynamic importance of this H-bonding network, this study focuses on the individual replacement of Thr17 and Thr82 with alanine, effectively altering the key H-bonding interactions that connect loop 1 and His48 to the rest of the protein. ^{15}N CPMG dispersion studies, nuclear magnetic resonance (NMR) chemical shift analysis, and NMR line shape analysis of point mutants T17A and T82A demonstrate that the evolutionarily conserved single H-bond linking His48 to Thr82 is essential for propagating ms motions from His48 to the active site of RNase A on the time scale of catalytic turnover, whereas the T17A mutation increases the off rate and conformational exchange motions in loop 1. Accumulating evidence from our mutational studies indicates that residues experiencing conformational exchange in RNase A can be grouped into two separate clusters displaying distinct dynamical features, which appear to be independently affected by mutation. Overall, this study illuminates how tightly controlled and finely tuned ms motions are in RNase A, suggesting that designed modulation of protein motions may be possible.

Ribonuclease A (RNase A),[1] like many enzymes, utilizes molecular motions during its conversion of substrate to product (*1*). In RNase A, the rate-limiting step for its rapid cleavage of single-stranded RNA is the product release step, which includes a conformational change in the enzyme itself (*2*, *3*). These enzyme motions occur on the millisecond (ms) time scale, as first elucidated from temperature jump experiments in the mid-1960s (*2*, *4*−*9*). These equilibrium perturbation experiments detected a pH-dependent motion in RNase A that occurred with a frequency of 10^3 s^{-1}. On the basis of the pH dependence and solvent isotope effects for this motion, in addition to the measurement of its activation enthalpy, Hammes and co-workers predicted that a solvent-exchangeable hydrogen atom associated with a histidine residue was integral to the observed motion in RNase A. Subsequent nuclear magnetic resonance (NMR) studies implicated histidine 48 as the residue involved in this conformational motion on the basis of the observed discontinuity of chemical shift changes during pH titrations (*10*−*12*). The three-dimensional structure of RNase A showed that His48 was not located at the enzyme active site but rather ∼18 Å distant with its imidazole side chain partially sequestered from solvent and positioned in a region primarily composed of residues from loop 1, which connects α-helix 1 with α-helix 2 (Scheme 1) (*13*). The molecular details of how His48 is involved in the rate-limiting product release step (*14*) have largely gone unresolved.

Advances in solution NMR techniques for characterizing ms time scale molecular motions (*15*) and the ability to readily incorporate site specific changes at individual amino acid sites have allowed further investigation of the role of motions in RNase A function. Initial NMR CPMG relaxation dispersion studies of uniformly ^{15}N-labeled apo-RNase A showed that multiple residues located throughout RNase A were involved in a ms conformational exchange process and that the time scale of this motion closely matched the overall catalytic turnover rate (*16*). These results suggested that motions in RNase A were more widespread than just the immediate area surrounding His48. Given the numerous residues involved in this motion, it was not initially clear that His48 was indeed the cause of the motions in RNase A. However, subsequent pH studies of this motion (unpublished observations) did implicate a residue(s)

[†]N.D. acknowledges a postdoctoral fellowship from the Fonds Quebecois de la Recherche sur la Nature et les Technologies (FQRNT) from the Government of Quebec. J.P.L. acknowledges National Science Foundation Grants MCB-02236966 and MCB-0744161.

*To whom correspondence should be addressed. Phone: (203) 436-4847. Fax: (203) 432-6144. E-mail: patrick.loria@yale.edu.

[1]Abbreviations: 3′-CMP, cytidine 3′-monophosphate; ECP, eosinophil cationic protein; rcCPMG, relaxation-compensated Carr−Purcell−Meiboom−Gill; RNase A, ribonuclease A; RNase A-CO, codon-optimized ribonuclease A; WT, wild-type RNase A.

Published on Web 01/20/2011

Scheme 1: Hydrogen Bonding Interactions between His48 and Its Surrounding Environment in RNase A[a]

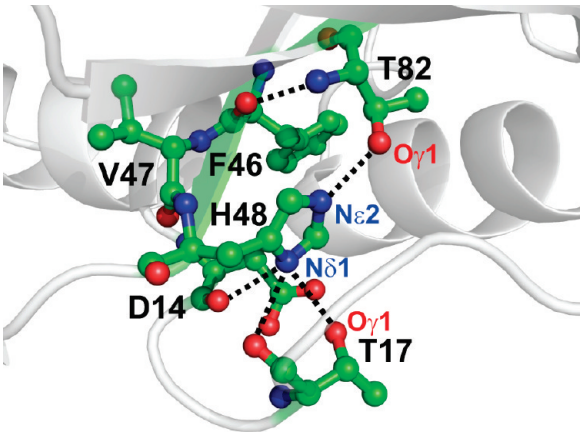

[a]Hydrogen bonds are shown as dashed lines, and atoms are displayed according to a standard coloring scheme: green for carbon, red for oxygen, and blue for nitrogen.

with a pK_a above 6.0 as being important for maintaining the observed motions. The rate of these motions was also found to be dependent on the deuterium content of the water solvent. This observed kinetic solvent isotope effect on protein motions (*17*), bolstered by additional proton inventory measurements, suggested that a single exchangeable proton was the source of these ms motions (*18*). Mutagenesis of His48 resulted in the loss of ms motions in the region surrounding His48, including loop 1, α1, α2, β1, β2, and β4 (*18*). In addition, exchange of loop 1 in RNase A for the shorter loop found in the RNase A homologue, eosinophil cationic protein (ECP), caused a similar loss of observable motions in the chimeric enzyme in these same regions (*19*). Thus, the majority of evidence to date implies that His48 plays an essential role in modulating the functional motions in RNase A.

Histidine 48 acts as a bridge that links loop 1 (residues 14−24), β-strand 1 on which His48 resides (residues 43−48), and β-strand 4 (residues 79−86) (Scheme 1). Both β1 and β4 comprise the B2 subsite of the enzyme's active site, forming the binding site for the pyrimidine portion of the single-stranded RNA (ssRNA) substrate. In the apoenzyme, a collection of hydrogen bonds links the imidazole side chain of His48 loop 1 and the B2 subsite (Scheme 1). The $N^{\varepsilon 2}$ group of His48 makes a H-bond with $O^{\gamma 1}$ of Thr82. On the other side of the imidazole ring, $N^{\delta 1}$ forms three interactions: one with $O^{\gamma 1}$ of Thr17, and two with the carbonyl oxygens of Thr17 and Asp14. In the 3′-CMP-bound product state, these interactions are maintained, although the distances are altered commensurate with the ∼1 Å shift of loop 1, and an additional interaction between $N^{\varepsilon 2}$ of His48 and the side chain of Gln101 is formed. These multiple interactions stand in some contrast to the linear NMR proton inventory experiments that suggested a single important hydrogen bond was involved in the motion in RNase A (*18*). However, analysis of 266 RNase A sequences revealed that His48 is 86% conserved (*20*). Moreover, when His48 is present, a threonine also is found at position 82. In contrast, Thr17 is only 17% conserved among these ribonucleases, suggesting that the coexistence of the His48−Thr82 pair is a more stringent requirement for function. To further investigate the importance of the hydrogen bonding network involving His48, we individually mutated Thr82 and Thr17 to alanine and studied the ms motions and product analogue binding in comparison to those of wild-type RNase A (WT). Our results show that the single His48 ($N^{\varepsilon 2}$)−Thr82 ($O^{\gamma 1}$) H-bond is mandatory for the propagation of WT ms dynamics and uncouples loop 1 dynamics from the remainder of the protein in mutant T82A. In contrast, while still considerably destructive, removal of the single $N^{\delta 1}$−$O^{\gamma 1}$ H-bond linking Thr17 to His48 allows for the partial conservation of ms dynamics in variant T17A. This mutational disruption of enzyme motion offers new insights pertaining to the importance of H-bonding interactions in the propagation of functional motions in proteins, opening the door to the potential allosteric modulation of enzyme activity by mutagenesis.

MATERIALS AND METHODS

DNA Constructs. Oligonucleotide synthesis and DNA sequencing were performed by the W. M. Keck Foundation Biotechnology Resource Laboratory (Yale University), and the wild-type, 372 bp bovine RNase A gene was codon-optimized (RNaseA-CO) by GenScript (Piscataway, NJ) for enhanced expression in *Escherichia coli*. The RNaseA-CO gene was PCR-amplified with terminal primers NDEIRACOF (5′-CACACACATATGAAAGA AACCGCGGCGGCCAAA-3′) and RACOHINDR (5′-CACACAAAGCTTTTATTACACGCTC GCATCAAAATGCAC-3′) to remove the pELB leader sequence and to introduce the 5′ and 3′ restriction sites *Nde*I and *Hin*dIII, respectively. The recombinant gene was subsequently digested with *Nde*I and *Hin*dIII, subcloned into the *Nde*I- and *Hin*dIII-digested pET22b(+) expression vector (EMD Chemicals, San Diego, CA), and transformed into *E. coli* XL10-Gold cells (Stratagene, La Jolla, CA). This pET22b(+)-RNaseA-CO construct served as a template for all subsequent DNA substitutions. The T17A and T82A mutations were introduced by the QuikChange Site-Directed Mutagenesis Kit (Stratagene) using RACOT17AF/RACOT17AR (5′-CAGCACATGGATAGCA-GCGCGAGCGCGGCGAGCAGCAGC-3′/5′-GCTGCTGC-TCGCCGCGCTCGCGCTGCTATCCATGTGCTG-3′) and RACOT82AF/RACOT82AR (5′-GCTATAGCACCATGAGC ATTGCGGATTGTCG CGAAACCGGCAGC-3′/5′-GCTG-CCGGTTTCGCGACAATCCGCAATGCTCATGGTGCTA-TAGC-3′) primer pairs, respectively.

Protein Expression, Refolding, and Purification. To reduce toxicity effects caused by the overexpression of RNase A, expression of mutants T17A and T82A was performed in *E. coli* C41(DE3) cells (Lucigen, Middleton, WI). Isotopically ^{15}N-labeled RNase A mutants T17A and T82A were expressed, refolded, and purified according to a previously optimized protocol (*19*).

Solution NMR Experiments. All NMR experiments were performed at 298 K as calibrated with a standard methanol sample (*21*) on Varian NMR spectrometers equipped with triple-resonance probes and pulsed-field gradients. A 773 μM ^{15}N-labeled sample of RNase A-T17A and an 830 μM ^{15}N-labeled sample of RNase A-T82A were used to perform all the relaxation experiments and the 3′-CMP titration experiments. Relaxation-compensated Carr−Purcell−Meiboom−Gill (rcCPMG) experiments (*15*) were performed as described previously (*19*) on ligand-free enzymes at magnetic fields of 11.7, 14.1, and/or 18.8 T. Resonance assignments for mutant enzymes were initially based on comparison with wild-type chemical shifts and verified with a ^{1}H−^{15}N TOCSY-HSQC experiment (*22*).

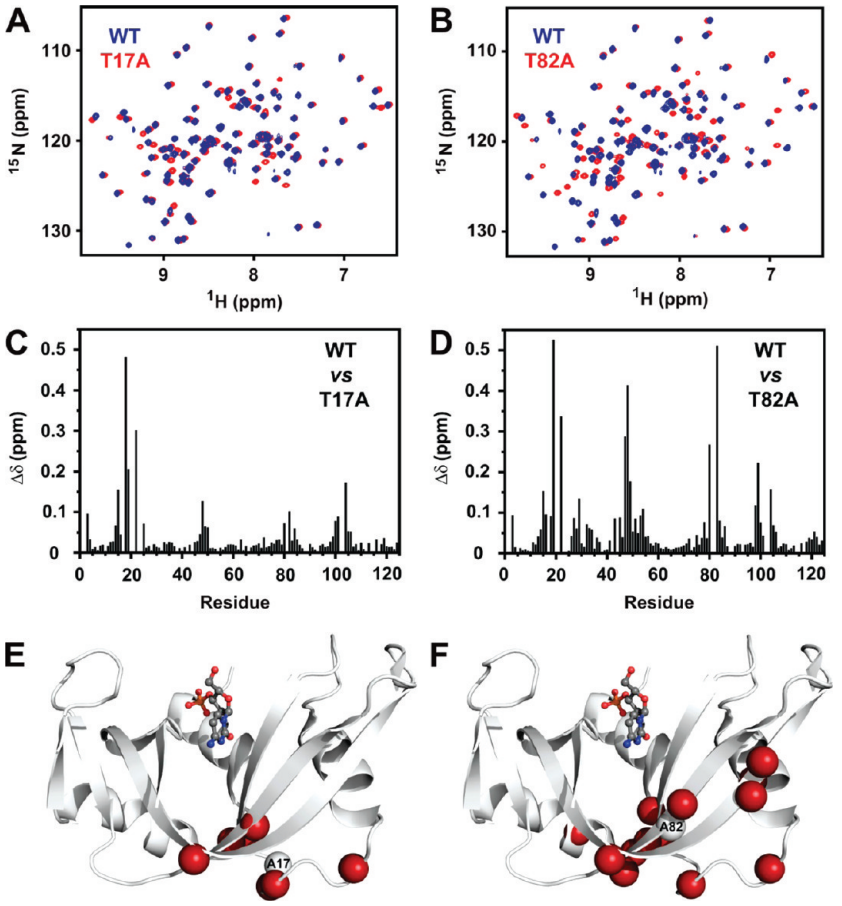

FIGURE 1: Chemical shift variations caused by the T17A and T82A mutations in RNase A. (A) Overlay of ^{15}N HSQC spectra for WT (blue) and RNase A-T17A (red). (B) Overlay of ^{15}N HSQC spectra for WT (blue) and RNase A-T82A (red). (C and D) Composite chemical shift differences for WT vs T17A (C) and WT vs T82A (D) shown as a function of amino acid sequence. (E and F) Mapping of $\Delta\delta$ for WT vs T17A (E) and WT vs T82A (F) on the three-dimensional structure of RNase A (Protein Data Bank entry 1RPF). Residues with $\Delta\delta$ values of > 0.1 ppm are represented as red spheres; the site of mutation is shown as a white sphere, and 3′-CMP is shown in ball-and-stick representation. Chemical shift variations are a composite of amide ^{1}H and ^{15}N chemical shift values calculated according to the relationship $\Delta\delta = [(\delta_{HN}^2 + \delta_N^2/25)/2]^{1/2}$, in which $\Delta\delta$ is the difference in chemical shift between the two proteins for amide $^{1}H^{N}$ and $^{15}N^{H}$ nuclei (*33*). ^{15}N HSQC spectra were recorded at 14.1 T, 298 K, and pH 6.4.

CPMG dispersion data for WT were fit as described previously (*23*). For CPMG data with T17A, all residues were in the fast-exchange regime and so were analyzed using the fast-limit equation as described previously (*24*). ϕ_{ex} ($p_A p_B \Delta\omega^2$), in which p_A and p_B are the equilibrium site populations for conformations A and B, respectively, and $\Delta\omega$ is the chemical shift difference for an individual nucleus between conformations A and B, was determined. For residues in the fast limit of conformational exchange, ϕ_{ex} is determined directly from the fits, whereas for residues in intermediate to slow exchange, ϕ_{ex} is obtained directly from the product of the individual values.

3′-CMP Titration Experiments. The kinetics of the binding interaction of 3′-CMP with RNase A mutants T17A and T82A were measured by titration of 3′-CMP as previously published (*19*, *23*, *25*), where ^{15}N HSQC spectra were recorded for titration points corresponding to 3′-CMP:enzyme molar ratios of 0, 0.174, 0.393, 0.691, 1.31, 2.71, 6, and 12. These two-dimensional experiments were conducted with 256 t_1 and 8192 t_2 points with proton and nitrogen spectral widths of 1600 and 7000 Hz, respectively. NMR line shape analysis was performed using *BiophysicLab* developed in the Kovrigin laboratory at the Medical College of Wisconsin (http://biophysicslab.net/). In brief, the one-dimensional spectral slices from the NMR two-dimensional HSQC series from titrations were exported using the *BiophysicsLab* extension for *Sparky* spectral processing software (http://www.cgl.ucsf.edu/home/sparky/). Fitting of a series of one-dimensional slices for each individual residue was performed using *BiophysicsLab* in the following steps: (1) normalization of the peak area to remove broadening in the orthogonal dimension, (2) fitting of the initial and final traces to Lorentzian line shapes to determine an initial guess for peak positions and line widths, and (3) fitting of the full titration series with the Bloch−McConnell equations [describing exchange between free and ligand-bound states of the protein (*25*, *26*)] to determine the ligand dissociation rate constant (k_{off}), the equilibrium dissociation constant (K_d), and the frequency and line width of the bound state. Detemination of 95% confidence intervals for the fitting parameters was performed utilizing the Monte Carlo approach. A common correction to the molar ratio of the ligand to the protein in the NMR sample was also optimized to account for the limited accuracy of the protein concentration as well as the small uncertainty in the ligand absorption coefficient. After every individual peak had been fit, the global fitting session was performed where all data sets for a specific form of RNase A (WT, T17A, or T82A) were fit to common values of k_{off}, K_d, and the correction to ligand:protein molar ratio, while optimizing individual frequencies and line widths of the bound complex for every peak. A small residual deviation of the fitted curves from

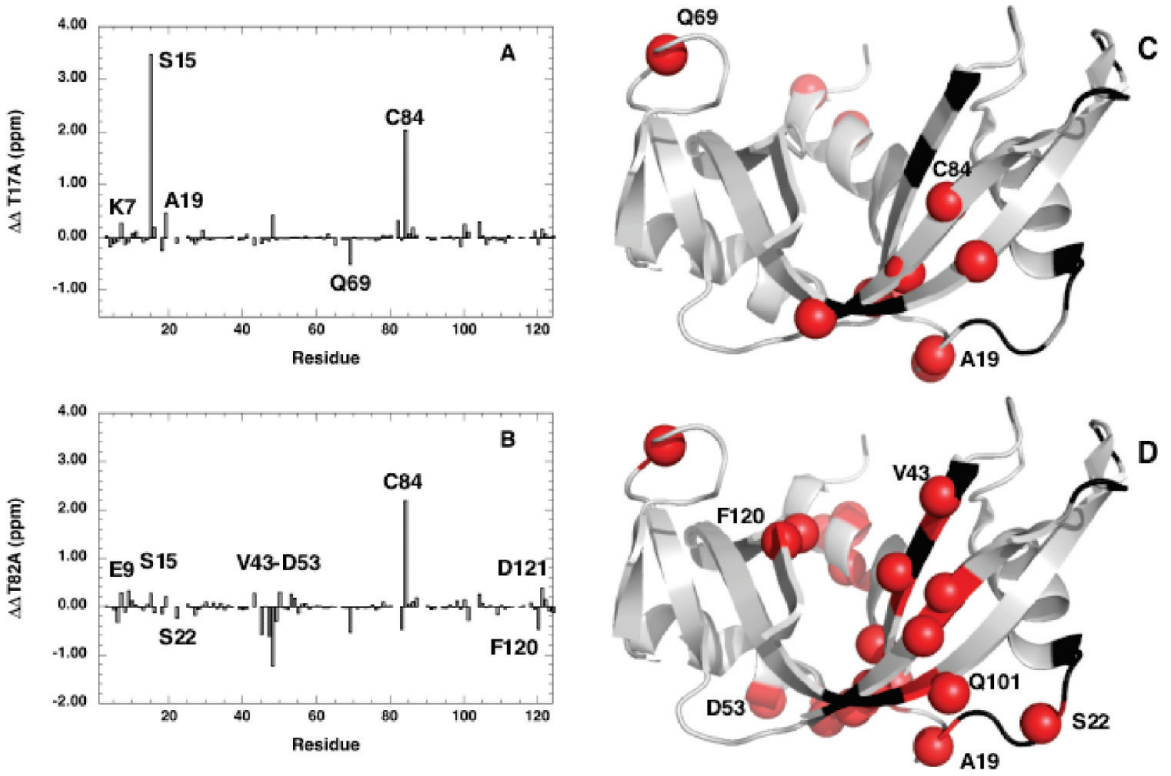

FIGURE 2: Effects of mutations on product analogue binding. The alteration in the response of RNase A to binding 3′-CMP is shown for (A and C) T17A and (B and D) T82A. In panels A and B, the chemical shift difference between the apoenzyme and the 3′-CMP-bound enzyme is shown as a function of amino acid residue, in which $\Delta\Delta = (\delta_{WT}^{apo} - \delta_{WT}^{CMP}) - (\delta_{mutant}^{apo} - \delta_{mutant}^{CMP})$, where δ is the residue specific ^{15}N chemical shift in the presence and absence of 3′-CMP for WT and mutant RNase A enzymes. $\Delta\Delta$ then represents the deviation of the mutant's interaction with CMP compared to that of WT. In panels C and D, $\Delta\Delta$ values of greater than ± 0.2 ppm are shown on the RNase A structure as red spheres; unassigned or overlapped residues are colored black.

experimental data was noted, which possibly originates from NMR instrument drift during the titration series. However, peak positions and widths were reproduced reasonably well, making it possible to perform a quantitative comparison between RNase A variants.

RESULTS AND DISCUSSION

Chemical Shift Assignments. The $^{1}H-^{15}N$ chemical shifts of both mutants are similar to those of WT (Figure 1). This similarity along with results from the TOCSY-HSQC analysis allowed assignment of 97 and 96% of assigned WT residues for T17A and T82A, respectively. Unassigned residues in each mutant that are assigned in WT are Asn44 and Gln103 for T17A and Thr17, Asn44, and Asn103 for T82A. In addition, Ala17 and Ala82 are unassigned in each mutant enzyme. Unassigned WT residues Glu2, Ala20, and Ser21 are well-resolved in both T17A and T82A. In T17A, Thr82 is assigned, whereas in T82A, Thr17 is not assigned. The lack of an assignment for Thr17 in the T82A mutant may be a result of the larger effects caused by mutation of Thr82 relative to Thr17 (vide infra). The average chemical shift differences between T17A and WT and between T82A and WT are 0.04 ± 0.06 ppm ($n = 106$) and 0.06 ± 0.09 ppm ($n = 105$), respectively. The sites of chemical shift differences from the WT enzyme are shown as a function of residue in Figure 1C,D and mapped onto the structure in Figure 1E,F. These data indicate that both mutants fold properly and are structurally very similar to the WT enzyme.

Differential Interaction with a Ligand. To assess the similarities to WT with respect to ligand binding, we analyzed the chemical shift changes for WT, T17A, and T82A upon binding the product analogue 3′-CMP. For most residues in both mutant enzymes, the magnitude and direction of the ^{15}N chemical shift changes upon 3′-CMP binding are similar to those observed for WT (Figure 2), suggesting that both mutant enzymes experience electrostatic and conformational changes similar to those of the WT enzyme when it encounters 3′-CMP. However, for T17A and T82A, there are several residues that display significant differences in their response to 3′-CMP binding (Figure 2). These differences from WT are more pronounced for the T82A mutant than for the T17A enzyme, indicating that mutation of Thr82 is a more disruptive one with respect to ligand binding than the Thr17 mutation. Alterations in loop 1 upon interaction with 3′-CMP are evident in both mutants. Furthermore, Asp83 and Cys84, near the Thr82 site, and Gln69 also display differences with respect to WT behavior. However, in the T82A enzyme, additional differences are also observed between β4 residues 43−53 and Phe120 and Asp121 (Figure 2), in which these latter two residues are located at the catalytic site and residues in β4 form the B2 subsite. Thus, the T82A mutation additionally alters how the residues around His48 respond to binding of 3′-CMP, an effect that also appears to propagate to longer distances, reaching Phe120 and Asp121, which are 12 Å distant but contact the phosphate group of the 3′-CMP ligand. This effect of altered product-induced chemical shift changes was also observed in the H48A and loop 1 chimera enzymes studied previously (*18*, *19*). Thus, it appears that alanine at position 82 alters the ability of RNase A to undergo ligand-induced changes as does complete removal of His48 (*18*).

NMR line shape analysis of a 3′-CMP titration series with all three enzymes was performed to further investigate the kinetics of

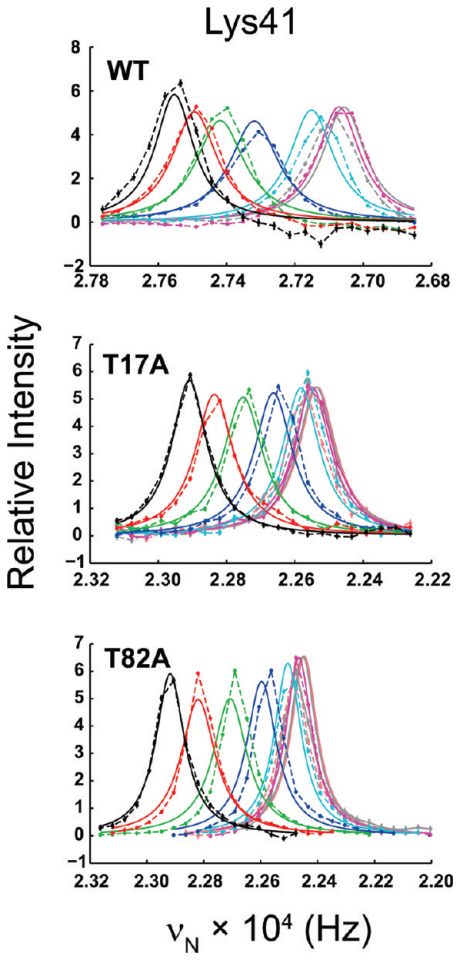

FIGURE 3: NMR line shape analysis of 3′-CMP binding. The titration curves of residue K41 are shown for WT, T17A, and T82A for 3′-CMP:enzyme molar ratios of 0 (black), 0.174 (red), 0.393 (green), 0.691 (blue), 1.31 (cyan), 2.71 (purple), 6 (pink, in only T17A and T82A), and 12 (gray). Best-fit curves obtained with *BiophysicsLab* (—) are superimposed on the experimental data (---).

Table 1: Interaction of 3′-CMP with WT, RNase A-T17A, and RNase A-T82A

enzyme	K_d (μM)	k_{off} (s^{-1})	k_{on} ($\times 10^8$ M^{-1} s^{-1})
WT	14 ± 4^a	2200 ± 100	1.57 ± 0.45
RNase A-T17A	100 ± 20	3100 ± 260	0.31 ± 0.07
RNase A-T82A	120 ± 25	2200 ± 260	0.18 ± 0.04

[a]Uncertainties determined from a Monte Carlo estimation.

interaction of the 3′-CMP product analogue with RNase A. For WT, the value for the dissociation rate constant (k_{off}) that we obtain from line shape analysis is 2200 ± 60 s^{-1} and is in agreement with previously determined values (*19*, *25*). For T82A, k_{off} equals 2200 ± 300 s^{-1} and is identical to the WT value, whereas for T17A, the value of k_{off} is slightly higher (3100 ± 300 s^{-1}) (Figure 3). For RNase A, the product release step is rate-limiting for the overall enzymatic reaction (*3*). The line shape data here suggest that mutation of Thr82 has no effect on this rate constant whereas mutation of Thr17 results in a slight elevation of the product analogue dissociation rate constant. Despite the similarities in the k_{off} values with that of WT, the mutants bind 3′-CMP between 7- and 10-fold weaker than WT. Thus, these mutations primarily elicit their effects via decreases in k_{on} (Table 1), perhaps because of their disruption of the active site structure and dynamics. For T82A, these data suggest that ms protein motions are uncoupled from product dissociation, unlike the case with WT in which motion and product release are concerted.

Conformational Exchange Motions. We previously investigated the ^{15}N backbone dynamics and functional effects of various mutations in RNase A and found that residues experiencing conformational exchange motions can be grouped into two separate clusters showing distinct dynamical features and distinct sensitivity to solvent ^2H content as summarized in Figure 4 (*18*). Millisecond motions in cluster 1 are sensitive to the deuterium content of the solvent and encompass several residues in the α2, β1, β2, β4, and loop 1 regions. In contrast, cluster 2 consists of residues of loop 4 and β2, and the observed millisecond motions in this region are insensitive to ^2H solvent isotope. These two clusters of residues are separated by the active site cleft and form two structurally distinct regions of the protein (Figure 4). In addition, the chemical exchange behavior of each cluster appears to be independently affected by mutation. For example, replacement of cluster 2 residue Asp121 with alanine affects the dynamic behavior of all of cluster 2 but does not influence the conformational exchange of cluster 1 residues (*25*). Conversely, replacements of Thr82 (this study), His48 (*18*), and loop 1 (*19*), all of which are located in cluster 1, almost completely abolish conformational exchange motions for residues of cluster 1 yet cause insignificant changes to the millisecond motions of cluster 2 (Figure 4).

Interestingly, despite being nearly 20 Å from the active site, His48 was found to be a key modulator in coupling protein motion with enzyme function, a result that was attributed to the involvement of the side chain imidazole of His48 (Figure 4 and Scheme 1) (*18*). It was postulated that protonation and/or deprotonation of this imidazole side chain would act as a switch to facilitate the open-to-closed conformation of the enzyme by connecting motions, which occur on the time scale of catalytic turnover, from loop 1 to β1, β2, and β4 through His48. Replacement of His48 with alanine completely abolishes conformational exchange in RNase A, as does replacing the entire loop 1 of RNase A (residues 14−25) with the shorter loop 1 of the human homologue ECP (Figure 4) (*19*). To further evaluate the importance of the hydrogen bonding network involving His48 and its surrounding local environment in the millisecond motions in RNase A, we investigated molecular motions on this time scale by ^{15}N CPMG relaxation NMR dispersion experiments (*15*) with WT, T17A, and T82A.

In a fashion similar to that for all other prior mutations in this region, replacement of Thr82 with alanine eliminates the positive CPMG relaxation dispersion curves, which are the hallmark of microsecond to millisecond motions for many residues of cluster 1. These results are similar to what is observed for the H48A and RNase A_{ECP} enzymes (Figure 5A−C) (*18*), further confirming the importance of the hydrogen bonding interaction between His48 and Thr82 in propagating motions throughout cluster 1 (*27*−*31*). The importance of this interaction is underscored by the coevolution of these two residues in RNase A sequences, as noted above. Further inspection indicates that the motions in loop 1 and for some surrounding residues are not abolished in the T82A mutant but rather shifted to a different time scale compared to those in WT (Figure 6). In the T82A enzyme, the transverse relaxation rates (R_2 for τ_{cp} = 0.625 ms) are

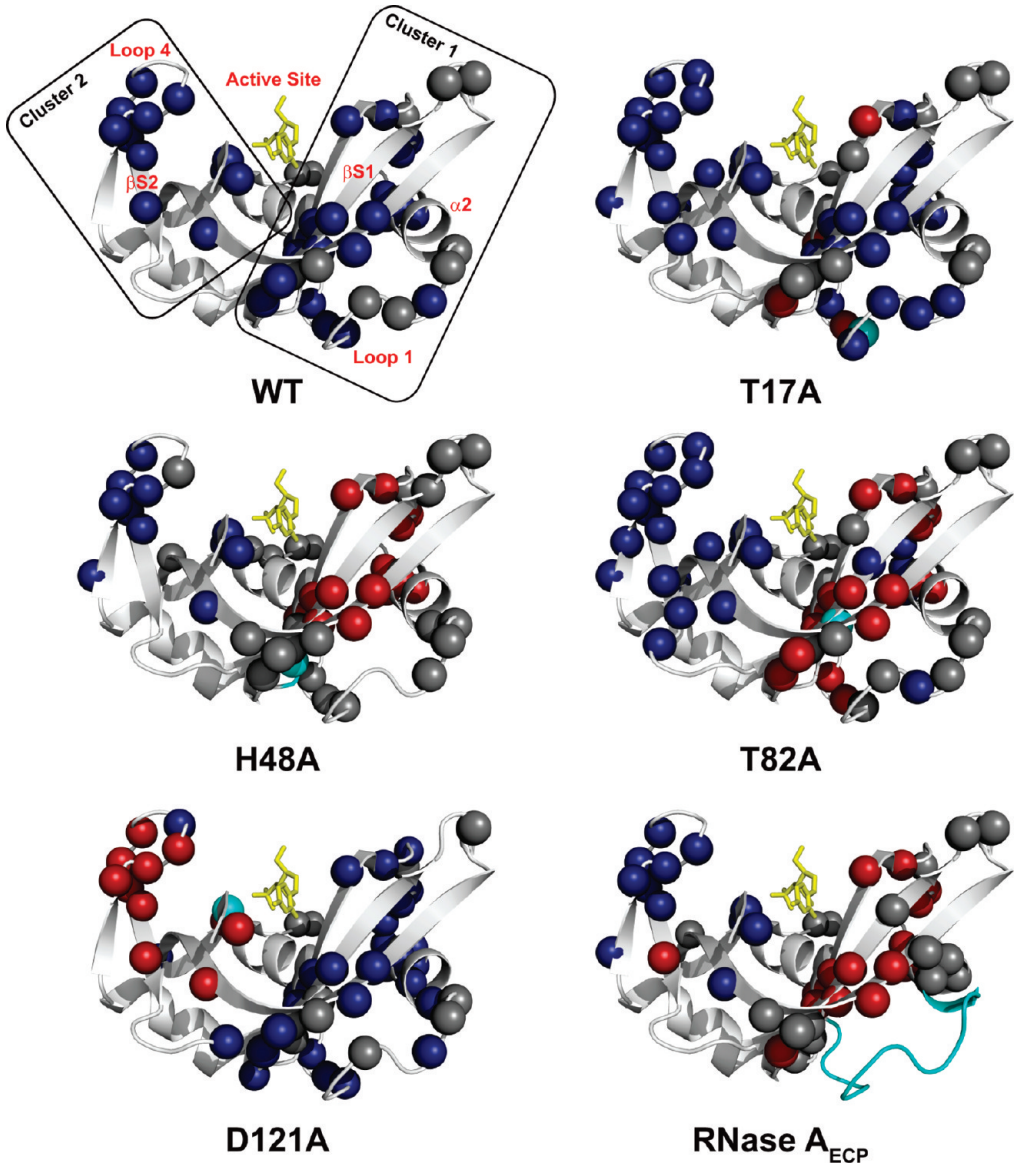

FIGURE 4: Effect of mutation on microsecond to millisecond dynamics in RNase A. Residues with ^{15}N CPMG dispersion profiles are depicted as blue spheres. Residues with no chemical exchange relative to WT (i.e., residues that lost microsecond to millisecond dynamics upon mutation) are depicted as red spheres. Unassigned residues are depicted as gray spheres. Secondary structure elements and clusters discussed in the text are highlighted on the structure of WT (Protein Data Bank entry 1RPF). The site of mutation is colored cyan, and 3′-CMP is shown as yellow sticks.

significantly elevated for several residues compared to those of their WT and T17A counterparts. The elevated rates in T82A indicate the presence of microsecond to millisecond motions that are not suppressed even at the fastest CPMG pulsing rates employed in the relaxation dispersion experiment. The inability to suppress the effects of molecular motions on the observed R_2 value by a CPMG pulse train suggests the motions are occurring on a time scale faster than $3.2/\tau_{cp}$ (*32*), where τ_{cp} is the delay between CPMG 180° pulses. For these experimental conditions, this would indicate that molecular motion is faster than approximately 5000 s^{-1}. This value is compared to ~2000 s^{-1}, which is the observed exchange rate constant for motions in WT (*16*). As one can see in Figure 6, these regions of elevated transverse relaxation rates are localized to loop 1 and not the remainder of cluster 1. This suggests that mutation of Thr82 not only accelerates motions in loop 1 but also uncouples loop 1 motions from the remainder of the protein, effectively cutting off the flow of motion to the active site region. The latter effect evidently reduces the affinity of the enzyme for 3′-CMP by decreasing k_{on}; in other words, mutation of Thr82 uncouples the loop 1 motions with residues in the enzyme active site.

In contrast to T82A, the mutation at position 17 does not significantly alter the R_2 values at τ_{cp} = 0.625 ms from their WT values (Figure 6), suggesting a similar time scale of motions in T17A and WT. Moreover, the dispersion curves for T17A are similar to that of WT, though with some interesting differences. The replacement of Thr17 with alanine has a significant effect on the dynamics of cluster 1 residues. Conformational exchange for residues Ala5, Gln11, Ser15, Ser18, Ser22, Met30, Ser32, Asn34, Leu35, Phe46, and Val47 remains with a k_{ex} of 3200 ± 350 s^{-1}, based on a global analysis of CPMG data at 600 and 800 MHz. The exchange rate constant for motions in T17A is 1.6-fold higher than it is in WT. This measured value of k_{ex} is similar to the k_{off} value for 3′-CMP measured from the line shape analysis indicating that motions around His48 and loop 1 remain coupled to the active site motions that participate in product release unlike what is observed in the T82A mutant. The role of Thr17 in this regard appears to be to maintain a reduced product

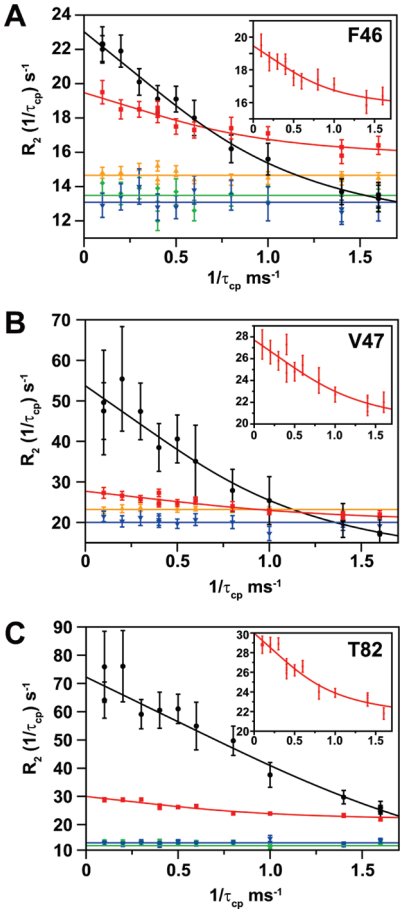

FIGURE 5: Conserved short-range conformational dynamics in mutant T17A. ^{15}N CPMG (14.1 T) dispersion curves of residues (A) F46, (B) V47, and (C) T82 for WT (black circles), RNase A-T17A (red squares), RNase A-T82A (orange triangles), RNase A-H48A (green diamonds) (*18*, *19*), and RNase A_{ECP} (blue inverted triangles) (*19*). Insets show close-ups of the RNase A-T17A data (same legend and axis labels).

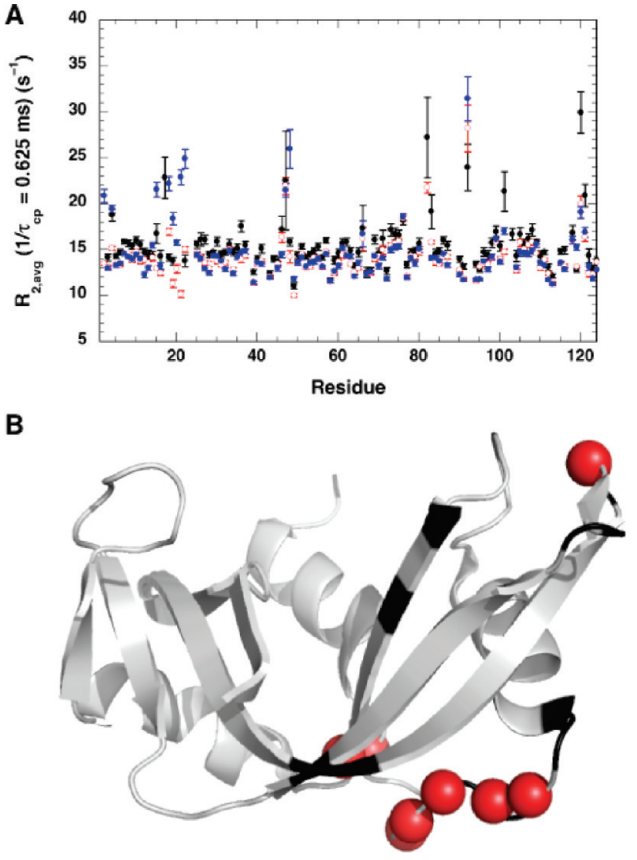

FIGURE 6: Effects of mutations on transverse relaxation rates (R_2). (A) Residue specific transverse relaxation rates ($R_{2,avg}$) equal $0.5(R_2^{in\text{-}phase} + R_2^{anti\text{-}phase})$, where $R_{2,avg}$ is the average of ^{15}N in-phase and antiphase transverse relaxation rates for WT (black), T17A (red), and T82A (blue). R_2 values were determined using a 40 ms constant relaxation time version of the relaxation-compensated CPMG experiment in which the delay between CPMG 180° refocusing pulses was set to 0.625 ms. (B) Residues in T82A with significantly elevated R_2 values are shown as red spheres mapped onto the structure of RNase A, with black regions corresponding to overlapped or unassigned residues. Experiments were performed at 14.1 T, 298 K, and pH 6.4.

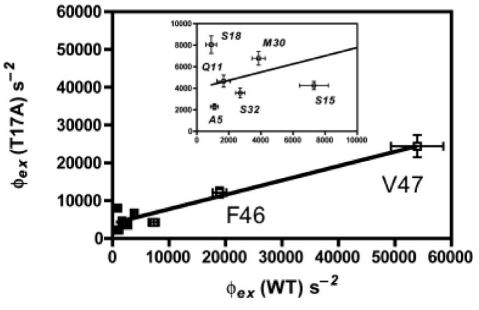

FIGURE 7: Comparison of dispersion parameters for WT and T17A. The correlation of ϕ_{ex} for WT and T17A for eight common residues is shown using the one-letter identification code for each. The inset is an expansion of the region in which $\phi_{ex} < 10000\ s^{-2}$. The line represents a best-fit linear regression to all the data points.

dissociation rate by maintaining slower protein motions. The functional reason, if any, for preserving slower motions is unclear.

Overall, these results are consistent with the linear proton inventory experiments probed by NMR relaxation dispersion methods that suggested a single dominant proton was important in these motions. On the basis of the results of this work, removal of the interaction between Thr82 and His48 has a large effect on protein motions, whereas removing the His48−Thr17 interaction has an only modest effect. The only interaction with the $N^{\varepsilon 2}$ position of His48 occurs via Thr82. In contrast, the T17A mutation retains two of three interactions with $N^{\delta 1}$ on the other side of the His48 imidazole ring (Scheme 1). Thus, mutation of Thr17 does not completely sever the connection of His48 with loop 1, but elimination of Thr82 cannot be overcome by other existing interactions. Nonetheless, the importance of Thr17 in RNase A motions should not be underestimated.

A comparison of ϕ_{ex} values for identical residues in WT and T17A gives a slope of 0.38, indicating that the amplitude of the motional effect is dampened in T17A (Figure 7). However, this slope is dominated by the data of Phe46 and Val47, and as seen in the inset of Figure 7, there are as many data points for which $\phi_{ex}^{T17A} > \phi_{ex}^{WT}$ as there are for which $\phi_{ex}^{T17A} < \phi_{ex}^{WT}$, indicating a nonuniform effect of mutation on the motional parameters, despite a correlation coefficient of 0.92 for these data. ϕ_{ex} in these plots equals the $p_a p_b \Delta\omega^2$ product that arises from the conformational exchange motion and its effect on the measured R_2. At present, it is not possible to know whether mutation of Thr17 causes a change in the equilibrium populations, $\Delta\omega$, or both. Whatever the mechanistic origins of the altered motions, it is not equally manifest in individual amino acid residues, yet the

kinetics of the conformational motion for all these residues in T17A are the same.

These studies illuminate how tightly controlled and finely tuned millisecond motions are in enzymes. Removal of a single, and lone, interaction between His48 and Thr82 abolishes millisecond motions in cluster 1 and shifts them toward the low microsecond regime. Deletion of the interaction between Thr17 and His48, which amounts to removal of one of the three total H-bonding interactions, slightly shifts the k_{ex} to a higher value for residues in cluster 1. In both cases, motions in cluster 2 are unaffected. Despite the sensitivity of the region surrounding His48 to perturbations, these studies do suggest that it may be possible to very selectively alter conformational dynamics and ligand binding for the purposes of rational protein design.

REFERENCES

1. Hammes, G. G. (2002) Multiple conformational changes in enzyme catalysis. *Biochemistry 41*, 8221–8228.
2. Cathou, R. E., and Hammes, G. G. (1964) Relaxation spectra of ribonuclease. I. The interaction of ribonuclease with cytidine 3′-phosphate. *J. Am. Chem. Soc. 86*, 3240–3245.
3. Park, C., and Raines, R. T. (2003) Catalysis by ribonuclease A is limited by the rate of substrate association. *Biochemistry 42*, 3509–3518.
4. Cathou, R. E., and Hammes, G. G. (1965) Relaxation spectra of ribonuclease. III. Further investigation of the interaction of ribonuclease and cytidine 3′-phosphate. *J. Am. Chem. Soc. 87*, 4674–4680.
5. del Rosario, E. J., and Hammes, G. G. (1969) Kinetic and equilibrium studies of the ribonuclease-catalyzed hydrolysis of uridine 2′,3′-cyclic phosphate. *Biochemistry 8*, 1884–1889.
6. Erman, J. E., and Hammes, G. G. (1966) Relaxation spectra of ribonuclease. IV. The interaction of ribonuclease with cytidine 2′:3′-cyclic phosphate. *J. Am. Chem. Soc. 88*, 5607–5614.
7. Erman, J. E., and Hammes, G. G. (1966) Relaxation spectra of ribonuclease. V. The interaction of ribonuclease with cytidylyl-3′:5′-cytidine. *J. Am. Chem. Soc. 88*, 5614–5617.
8. French, T. C., and Hammes, G. G. (1965) Relaxation spectra of ribonuclease. II. Isomerization of ribonuclease at neutral pH values. *J. Am. Chem. Soc. 87*, 4669–4673.
9. Hammes, G. G., and Walz, F. G. (1969) Relaxation Spectra of Ribonuclease. VI. Interaction of Ribonuclease with Uridine 3′-Monophosphate. *J. Am. Chem. Soc. 91*, 7179–7186.
10. Markley, J. L. (1975) Correlation proton magnetic resonance studies at 250 MHz of bovine pancreatic ribonuclease. I. Reinvestigation of the histidine peak assignments. *Biochemistry 14*, 3546–3554.
11. Markley, J. L. (1975) Correlation proton magnetic resonance studies at 250 MHz of bovine pancreatic ribonuclease. II. pH and inhibitor-induced conformational transitions affecting histidine-48 and one tyrosine residue of ribonuclease A. *Biochemistry 14*, 3554–3561.
12. Markley, J. L., and Finkenstadt, W. R. (1975) Correlation proton magnetic resonance studies at 250 MHz of bovine pancreatic ribonuclease. III. Mutual electrostatic interaction between histidine residues 12 and 119. *Biochemistry 14*, 3562–3566.
13. Kartha, G., Bello, J., and Harker, D. (1967) Tertiary structure of ribonuclease. *Nature 213*, 862–865.
14. Lee, G. C., and Chan, S. I. (1971) A ^{31}P NMR study of the association of uridine-3′-monophosphate to ribonuclease A. *Biochem. Biophys. Res. Commun. 43*, 142–148.
15. Loria, J. P., Rance, M., and Palmer, A. G. (1999) A Relaxation-compensated Carr-Purcell-Meiboom-Gill sequence for characterizing chemical exchange by NMR spectroscopy. *J. Am. Chem. Soc. 121*, 2331–2332.
16. Cole, R., and Loria, J. P. (2002) Evidence for flexibility in the function of ribonuclease A. *Biochemistry 41*, 6072–6081.
17. Kovrigin, E. L., and Loria, J. P. (2006) Characterization of the transition state of functional enzyme dynamics. *J. Am. Chem. Soc. 128*, 7724–7725.
18. Watt, E. D., Shimada, H., Kovrigin, E. L., and Loria, J. P. (2007) The mechanism of rate-limiting motions in enzyme function. *Proc. Natl. Acad. Sci. U.S.A. 104*, 11981–11986.
19. Doucet, N., Watt, E. D., and Loria, J. P. (2009) The flexibility of a distant loop modulates active site motion and product release in ribonuclease A. *Biochemistry 48*, 7160–7168.
20. Smith, B. D., and Raines, R. T. (2006) Genetic selection for critical residues in ribonucleases. *J. Mol. Biol. 362*, 459–478.
21. Cavanagh, J., Fairbrother, W. J., Palmer, A. G., Rance, M., and Skelton, N. J. (2007) Protein NMR Spectroscopy: Principles and Practice, 2nd ed., Elsevier Academic Press, San Diego.
22. Marion, D., Kay, L. E., Sparks, S. W., Torchia, D. A., and Bax, A. (1989) 3-dimensional heteronuclear NMR of N-15 labeled proteins. *J. Am. Chem. Soc. 111*, 1515–1517.
23. Beach, H., Cole, R., Gill, M. L., and Loria, J. P. (2005) Conservation of μs−ms enzyme motions in the apo- and substrate-mimicked state. *J. Am. Chem. Soc. 127*, 9167–9176.
24. Palmer, A. G., Kroenke, C. D., and Loria, J. P. (2001) Nuclear magnetic resonance methods for quantifying microsecond-to-millisecond motions in biological macromolecules. *Methods Enzymol. 339* (Part B), 204–238.
25. Kovrigin, E. L., and Loria, J. P. (2006) Enzyme dynamics along the reaction coordinate: Critical role of a conserved residue. *Biochemistry 45*, 2636–2647.
26. McConnell, H. M. (1958) Reaction Rates by Nuclear Magnetic Resonance. *J. Chem. Phys. 28*, 430–431.
27. de Mel, V. S., Doscher, M. S., Martin, P. D., and Edwards, B. F. (1994) The occupancy of two distinct conformations by active-site histidine-119 in crystals of ribonuclease is modulated by pH. *FEBS Lett. 349*, 155–160.
28. Fontecilla-Camps, J. C., de Llorens, R., le Du, M. H., and Cuchillo, C. M. (1994) Crystal structure of ribonuclease A d(ApTpApApG) complex. Direct evidence for extended substrate recognition. *J. Biol. Chem. 269*, 21526–21531.
29. Kovrigin, E. L., Cole, R., and Loria, J. P. (2003) Temperature dependence of the backbone dynamics of ribonuclease A in the ground state and bound to the inhibitor 5′-phosphothymidine (3′-5′) pyrophosphate adenosine 3′-phosphate. *Biochemistry 42*, 5279–5291.
30. Leonidas, D. D., Chavali, G. B., Oikonomakos, N. G., Chrysina, E. D., Kosmopoulou, M. N., Vlassi, M., Frankling, C., and Acharya, K. R. (2003) High-resolution crystal structures of ribonuclease A complexed with adenylic and uridylic nucleotide inhibitors. Implications for structure-based design of ribonucleolytic inhibitors. *Protein Sci. 12*, 2559–2574.
31. Leonidas, D. D., Shapiro, R., Irons, L. I., Russo, N., and Acharya, K. R. (1997) Crystal structures of ribonuclease A complexes with 5′- diphosphoadenosine 3′-phosphate and 5′-diphosphoadenosine 2′-phosphate at 1.7 Å resolution. *Biochemistry 36*, 5578–5588.
32. Allerhand, A., and Gutowsky, H. S. (1965) Spin-echo studies of chemical exchange. II. Closed formulas for two sites. *J. Chem. Phys. 42*, 1587–1599.
33. Grzesiek, S., Stahl, S. J., Wingfield, P. T., and Bax, A. (1996) The CD4 determinant for downregulation by HIV-1 Nef directly binds to Nef. Mapping of the Nef binding surface by NMR. *Biochemistry 35*, 10256–10261.